

Laser-Induced Fluorescence Measurements of a Turbulent Plume

D. R. Webster, M.ASCE¹; S. Rahman²; and L. P. Dasi³

Abstract: The laser-induced fluorescence (LIF) measurement technique is discussed in the context of environmental fluid mechanics. The measurement equipment and procedures employed in our laboratory are described in detail. The technique is applied to an isokinetic chemical plume (neutrally buoyant) in a turbulent open channel flow. A nonuniform laser sweep rate is employed to take full advantage of the dynamic range of the digital camera over the entire spatially varying concentration field. Statistical measures of the concentration field, such as the average and variance, are presented and discussed. Comparisons are made with theoretical models and previous experimental observations. The plume width grows at a greater rate in the downstream direction than that predicted by the analytical model of a point source release into a uniform flow. Probability density function distributions do not resemble Gaussian distributions, which reflects the highly intermittent nature of the concentration time record. The current measurements suggest that LIF is a valuable technique for nonintrusively recording the scalar field evolution in turbulent flows.

DOI: 10.1061/(ASCE)0733-9399(2003)129:10(1130)

CE Database subject headings: Flow measurement; Plumes; Measuring instruments.

Introduction

Turbulent mixing of passive quantities, such as chemical species, is important in the context of many environmental flows. Example applications include control of water and air quality, regulation of hazards posed by the release of toxic or flammable materials, design of efficient mixing and combustion devices, and odor tracking strategies employed by aquatic and terrestrial animals. The focus of the current study is a chemical plume released isokinetically into a fully developed turbulent boundary layer in an open channel flow. This particular flow arrangement is motivated by studying the ability of benthic crustaceans (such as blue crabs) to track chemical odors to locate food and mates (Webster and Weissburg 2001). The arrangement is also relevant to sewage or contaminant release near riverbeds and pollution release in an atmospheric boundary layer (e.g., Fackrell and Robins 1982; Bara et al. 1992).

The objective of the experimental technique described in this paper is to quantify the spatial and temporal distribution of a passive chemical tracer in turbulent flows. The laser-induced fluorescence (LIF) measurement technique has been used in the recent past to quantify mixing in aqueous flows (e.g., Koochesfahani and Dimotakis 1985, 1986; Dahm and Dimotakis 1987;

Ferrier et al. 1993; Karasso and Mungal 1997; Chen and Jirka 1999; Crimaldi and Koseff 2001; Crimaldi et al. 2002). In addition, the LIF technique has been recently coupled with simultaneous velocity field measurements, performed via particle image velocimetry or a similar technique, to quantify the turbulent scalar flux (Sakakibara et al. 1997; Law and Wang 2000; Webster et al. 2001; Borg et al. 2001; Cowen et al. 2001). The basic principle of LIF is relatively simple. When fluorescence dye molecules are illuminated by a light source within the absorption spectrum of the dye, the molecules are excited to a higher state. The molecules emit light at a longer wavelength with intensity proportional to the incident light intensity and the dye concentration. Thus, by calibrating the incident light intensity (and other nonuniform effects) the instantaneous concentration at a point can be nonintrusively measured. In practice, a laser typically illuminates a plane in the flow and a digital camera system collects and records the emitted light. With the commercial availability of lasers, high-quality digital cameras, and timing control hardware, a LIF measurement system can be relatively inexpensively constructed.

This paper aims to describe the measurement techniques employed in our laboratory to measure the broad range of scales observed in turbulent scalar fields. The LIF equipment and procedures are described in detail. An example of environmental fluid mechanics application, namely a chemical plume, is discussed.

Experimental Setup

Fully developed, uniform open channel flow was established in a 1.07 m wide 24.4 m long tilting flume with a rectangular cross section and smooth bed. The experimental configuration is shown in Fig. 1. The temperature of the water was 20°C, and the average velocity in the flume was 50 mm/s. The flow depth, H was uniformly 200 mm to within 0.3 mm for at least 12 m approaching the measurement location. Previous measurements in this facility indicate that fully developed flow conditions can be established at

¹Associate Professor, School of Civil and Environmental Engineering, Georgia Institute of Technology, Atlanta, GA 30332-0355. E-mail: dwebster@ce.gatech.edu

²Graduate Research Assistant, School of Civil and Environmental Engineering, Georgia Institute of Technology, Atlanta, GA 30332-0355.

³Graduate Research Assistant, School of Civil and Environmental Engineering, Georgia Institute of Technology, Atlanta, GA 30332-0355.

Note. Associate Editor: Hamm-Ching Chen. Discussion open until March 1, 2004. Separate discussions must be submitted for individual papers. To extend the closing date by one month, a written request must be filed with the ASCE Managing Editor. The manuscript for this paper was submitted for review and possible publication on November 14, 2001; approved on August 23, 2002. This paper is part of the *Journal of Engineering Mechanics*, Vol. 129, No. 10, October 1, 2003. ©ASCE, ISSN 0733-9399/2003/10-1130-1137/\$18.00.

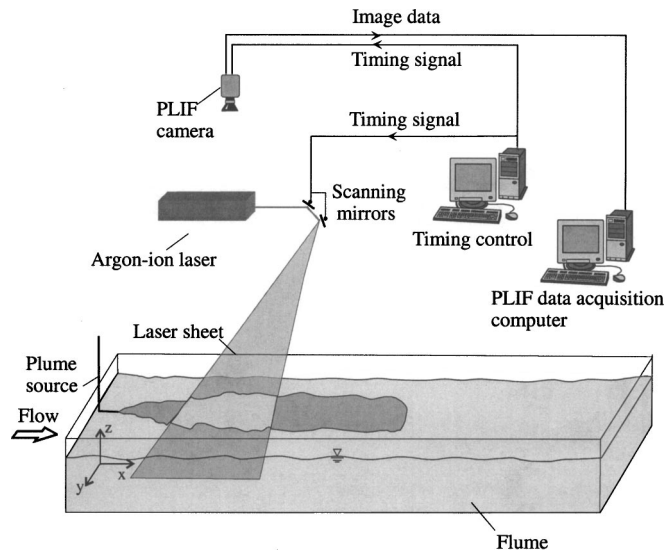


Fig. 1. Experimental apparatus

the measurement section (Tracy and Lester 1961). The boundary layer profile above the bed was measured (using laser Doppler velocimetry) and agreed well with the expected law-of-the-wall distribution in the range $30 < u^*z/\nu < 300$ (Fig. 2). The wall shear velocity, u^* , for the bed boundary layer was 3.55 mm/s.

The plume source consisted of a brass 4.7 mm diameter nozzle with a streamlined fairing to minimize the wake perturbation. The effluent was neutrally buoyant and the release velocity matched the channel flow velocity thus creating a passive, isokinetic source. The general features of the chemical plume released 25 mm above the bed can be seen in the photograph in Fig. 3. Dye released from the point source is advected downstream while turbulent fluctuations stir and spread the filaments. The dye distribution in the flow visualization image hints at the fact that the plume consists of small filaments of dye, interspersed within relatively clean water. The next section describes how the LIF technique is used to quantify the filamentous nature of the plume.

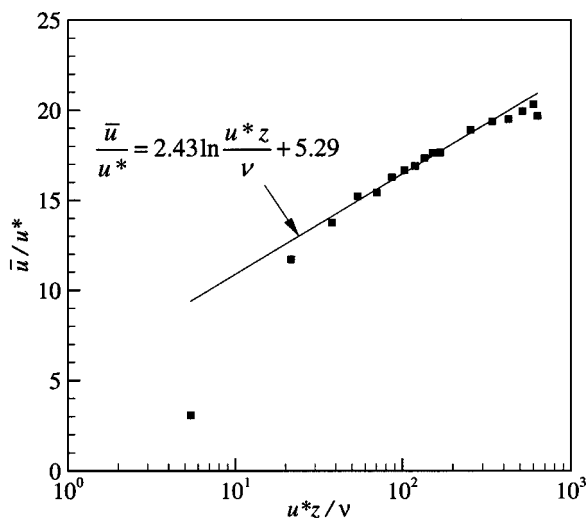


Fig. 2. Mean velocity profile [coefficients for law-of-the-wall profile are those recommended by Nezu and Rodi (1986), and wall shear velocity is 3.55 mm/s]



Fig. 3. Side view of a plume released isokinetically 25 mm (0.125H) above the bed into a fully developed turbulent boundary layer in an open channel flow

Measurement Technique

The LIF technique was used to record the long-time series of planar concentration fields with varying resolution. The LIF system is composed of a laser, a scanning mirror system, timing control, and an image acquisition system as shown in Fig. 1.

An argon-ion laser (5 W, Coherent Innova 90), tuned to 514 nm, was used to illuminate the flow. The laser beam entered the flume through glass sidewalls. It is extremely important to eliminate light reflected off solid surfaces in the measurement region because it causes false concentration measurements. Thus, the floor of the flume was painted flat black to provide a uniform nonreflecting background for the laser sheet. The peak absorption of the fluorescent dye, Rhodamine 6G, is at about 530 nm (Arcoumanis et al. 1990). The peak emission is in the yellow-orange wavelength range, around 560 nm. An optical cutoff filter (Tiffen color 21) blocked the laser light and passed only the fluoresced light to the camera sensor.

A Kodak MegaPlus ES 1.0 camera (8 bit, 1018 × 1008 pixels) viewed the measurement region from above. To eliminate optical distortion due to the free surface, a plexiglas sheet was half-submerged at the water surface in the photographic region. Observations in the flume and calculation of the boundary layer thickness (and the corresponding displacement thickness) suggest that the plexiglas sheet had a mild effect on the channel flow and plume (i.e., less than 2% perturbation to the channel velocity). By varying the camera mounting location and the focal length of the lens, two image resolutions were recorded. A Fujinon 12.5 mm focal length lens was used to record a large-scale region roughly 1 m × 1 m, and a Nikon MicroNikkor 200 mm focal length lens was used for a much smaller region, 20 mm × 20 mm. Planar measurements at the scale of 1 m present some unique challenges that will be discussed next [note that fields of similar dimension have been measured previously by Ferrier et al. (1993) at lower resolution]. The image resolution for each arrangement was determined by photographing a ruler located at the measurement plane. The respective resolutions for these images were approximately 1 mm and 0.02 mm per pixel. For the large-scale measurements, data were obtained at four overlapping regions at the same elevation as the nozzle ($z = 25$ mm). Between measuring each region, the plume source was moved 0.5 m upstream to ultimately record data up to 2.5 m downstream of the plume source. (Because the channel flow was fully developed, moving the plume source upstream is equivalent to moving the measurement station downstream.) The source concentration was increased for each successive downstream location such that the emitted light in the measurement region employed the full dynamic range of the camera. In addition, images of horizontal planes at 12 heights from the bed were collected for the region covering the first 1 m downstream of the source. The small-scale measurements were collected in the plane of the source, 1 m downstream.

The camera was connected to a Windows NT computer through a Coreco image capture board. The images were stored

on a hard drive array in real time using Video Savant software (IO Industries); a process referred to as real-time-to-disk. Thus, the length of the image sequence was limited only by the hard drive array capacity. This flow is highly intermittent and hence requires a very long measurement period to accurately resolve statistical quantities. For the data presented here, time series of 600 s were required for statistical convergence of the time average and standard deviation (Webster and Weissburg 2001). The camera was triggered at a rate of 10 Hz (6,000 samples) for data in the plane of the nozzle, and 5 Hz (3,000 samples) for other planes. Note that each image corresponds to 1 MB, thus a 6,000 image sequence results in a 6 GB file.

A lens focuses the laser beam in the measurement region; the beam thickness is 1 mm for the large-scale measurements and 0.1 mm for the small-scale measurements. Two mirrors mounted on galvanometers (Cambridge Technology) were used to position the beam horizontally and vertically. One mirror swept the laser beam in a plane parallel to the bed to create the laser sheet and the second mirror set the height of the sheet above the bed.

As can be inferred from Fig. 3, dilution was rapid with distance from the source for this plume. Thus, over a distance of 1 m, the concentration decreased dramatically (this is discussed quantitatively in the "Results" section). If a constant mirror sweep rate were employed, the near nozzle region would be bright due to relatively high local concentration. Conversely, the lower concentration filaments farther downstream would be extremely dim. To take full advantage of the dynamic range of the camera over the entire image, the sweep rate of the laser beam was nonuniform such that the incident light intensity increased with distance from the plume source.

To first-order approximation, the laser beam position is linearly related to the control voltage signal supplied to the rotating mirror

$$x = x_0 + \left(\frac{E - E_0}{E_1 - E_0} \right) (x_1 - x_0) \quad (1)$$

The objective of the following analysis is to specify the cyclic voltage signal pattern, E for the mirror to produce the desired nonuniform sweep rate. It is known that the emission intensity is linearly proportional to both the laser intensity and the species concentration (e.g., Koochesfahani and Dimotakis 1985). Thus, if we assume that the concentration decreases as a power law ($c \propto 1/x^n$), then the laser intensity should increase at the inverse rate ($I \propto x^n$) to produce uniform light emission. The local intensity of the laser light is proportional to the residence time of the beam, and thus inversely proportional to the beam velocity ($I \propto 1/v$). Combining these relations suggests that $v = dx/dt \propto 1/x^n$. Integrating this relationship and combining with Eq. (1) produces the functional form for the control voltage signal

$$E = E_0 + (E_1 - E_0) \left(\frac{t}{T} \right)^{1/(n+1)} \quad (2)$$

Nonuniform sweep rates were employed for the 1 m × 1 m fields. By trial and error, it was found that $n = 1.0$ produced the most uniform LIF images for the two fields closest to the source, and that $n = 0.5$ was best for the next two regions. Nonuniform sweep rates were not necessary for the small-scale measurements because the peak magnitude of the concentration varied mildly over the image field.

The timing control computer (Windows NT) provided the control voltage signals via a National Instruments multifunction input/output (I/O) board and the *LABVIEW* software. The I/O

board also sent a voltage trigger to the camera so that the electronic shutter was synchronized with the sweep.

Because of effects like laser sheet nonuniformity, lens vignette, and pixel response variability, a detailed calibration is critically important for quantitative measurements. Uniform dye concentrations were photographed *in situ* to provide the calibration data. Concentrated dye was injected upstream near the flume head box from a copper 38.1 mm diameter diffuser spanning the width of the flume with eight 1.6 mm diameter holes. A 20 mg/l solution of Rhodamine 6G was pumped through the diffuser. Varying the dye flow rate through the diffuser created the desired concentration levels in the flume. The turbulent jets through the diffuser holes and the ambient turbulence present in the channel flow mixed the dye to create a nearly uniform concentration distribution at the measurement region (over 20 m downstream of the diffuser). For each measurement arrangement, eighty images were captured for each of six concentration levels between 0 and 25 $\mu\text{g/l}$. To remove any slight nonuniformities in the dye distribution, the eighty images were averaged to produce a single calibration image for a given concentration level.

The calibration images were corrected for laser attenuation. The corrected intensity was calculated using the following equation (Ferrier et al. 1993):

$$I(i,j)_{\text{corrected}} = I(i,j)_{\text{measured}} \exp\{\alpha c L(i,j)\} \quad (3)$$

Ferrier et al. (1993) report that the value of the attenuation coefficient, α , for Rhodamine 6G is 0.0023 per $\mu\text{g/l}$ per mm. (The instantaneous plume images were not corrected for attenuation because the short optical path length through the dye filaments produced a negligible effect.)

The corrected calibration images were used to calculate a slope, $A(i,j)$, and intercept, $B(i,j)$, at each pixel location using a linear least-squares fit. In order to avoid misleading negative concentrations, the least-squares fit was forced to pass through the zero-concentration measurement. The raw images of the plume were subsequently converted to instantaneous concentration fields using the slope and intercept:

$$c(i,j) = A(i,j)I(i,j) + B(i,j) \quad (4)$$

Because the calibration was local for each pixel, all nonuniform effects such as the laser sweep rate, lens vignette, and pixel response variability were accounted for by the slope and intercept. The uncertainty for the instantaneous concentration measurements was estimated to be $\pm 3\%$ based on an analysis of the calibration procedure and measurement repeatability.

Turbulent Scales

The motivation for measuring the concentration field with the two image resolutions just described is to resolve the range of turbulent length scales expected in this flow. In this section, the relevant length scales are defined and estimated for the plume.

The range of scales for the velocity fluctuations extends from the integral scale down to the scale at which viscosity dissipates turbulent kinetic energy to heat. The integral scale, $l \sim H/2 = 100$ mm, is estimated as half of the channel depth, i.e., the largest eddies are physically constrained by the presence of the bed and free surface. The scale at which dissipation occurs is known as the Kolmogorov microscale and is estimated from the fluid viscosity and dissipation rate (Kolmogorov 1941):

$$\eta \sim \left(\frac{\nu^3}{\varepsilon} \right)^{1/4} \quad (5)$$

The dissipation rate is estimated by $\varepsilon \sim \bar{u}^3/l$, which comes from physical observations (Tennekes and Lumley 1972). The Kolmogorov microscale for this flow is estimated to be 0.7 mm. The corresponding Kolmogorov time scale, $\tau \sim (\nu/\varepsilon)^{1/2}$, is 0.5 s.

The length scales for the turbulent concentration field range from the plume width to the scale at which molecular diffusion acts to homogenize the distribution. This length scale is referred to as the Batchelor scale and is estimated from dimensional analysis as the square root of the ratio of the molecular diffusivity and the strain rate of the smallest velocity scales (Batchelor 1959)

$$L_B \sim \left(\frac{D}{\gamma} \right)^{1/2} \quad (6)$$

The strain rate of the smallest scales is proportional to the ratio of Kolmogorov velocity and length scales, $\gamma \sim v/\eta \sim (\varepsilon/\nu)^{1/2}$. Thus, the Batchelor length scale can be recast into a form that includes both the molecular diffusivity of the scalar and the kinematic viscosity:

$$L_B \sim \left(\frac{\nu D^2}{\varepsilon} \right)^{1/4} = \eta(\text{Sc})^{-1/2} \quad (7)$$

Eq. (7) also shows that the Batchelor and Kolmogorov length scales are related by the square root of the Schmidt number. The diffusivity of Rhodamine 6G in water is around $1 \times 10^{-9} \text{ m}^2/\text{s}$ (Crimaldi and Koseff 2001), therefore, the Batchelor scale is estimated to be 0.02 mm, which is 35 times smaller than the Kolmogorov microscale. Thus, we should expect a much finer structure for the concentration field than the velocity field. The corresponding time scale of the finest concentration variation observed at a point is $L_B/\bar{u} = 0.0004 \text{ s}$.

The resolution range of the plume images is 1 mm to 1 m for the large-scale measurements and 0.02 mm to 20 mm for the small-scale measurements. (Note that the sheet thickness for the small-scale measurements is 0.1 mm, thus limiting the measurement resolution in the vertical direction.) The small-scale measurements, therefore, can resolve the Batchelor scale in the photographic plane, while the large-scale measurements are coarser. The large-scale measurements, however, provide a broad perspective of the plume as it evolves in the downstream direction. Together the measurements span a large range of the length scales of this chemical plume.

Results

A photograph of the dye plume is shown in Fig. 3. The release location is in the logarithmic layer of the fully developed turbulent boundary layer (at $z^+ = z u^*/\nu = 90$). Because the effluent and channel velocities are matched, the velocity gradient produced by the release is very small and the production of turbulence due to velocity shear is minimal. Thus, stirring of the chemical tracer is mainly due to the turbulent fluctuations produced by the bed boundary layer. The plume exhibits evidence of stretching and folding processes that are normally associated with turbulent stirring. However, concentrated packets of dye are observed even at the end of the field of view, which suggests that the plume remains inhomogeneous.

One of the strengths of the planar LIF measurement technique is the ability to reveal the spatial distribution and variability. The contours of concentration shown in Fig. 4(a) reveal the high spatial variability of the plume. Note that the contour levels are nonlinearly spaced for Fig. 4(a). The measurement plane consists of the streamwise, x , and the spanwise, y , directions and the nozzle

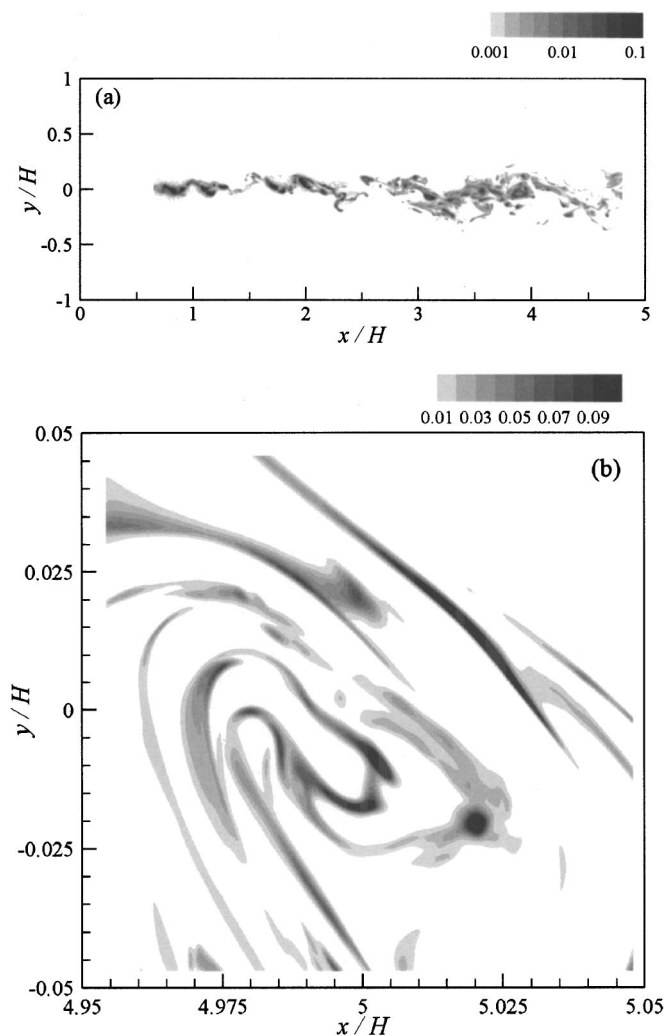


Fig. 4. (a) Large-scale and (b) small-scale measurements of instantaneous concentration field, c/C_o

is at the origin. The perspective for Fig. 4(a) is from above the flume (unlike Fig. 3, which was from the side). Data are not shown for $x/H < 0.6$ because the concentration peaks are beyond the linear calibration range in this region. The peak magnitudes decrease rapidly, dropping by roughly an order of magnitude between $x/H = 1$ and 4. This rapid decrease necessitates the nonlinear contour spacing in Fig. 4(a). The decrease in concentration results from molecular diffusion acting at the Batchelor scale on steep gradients created by turbulent stirring. The concentration gradients are very high in Fig. 4(a); the concentration rises from near zero to the peak value over very small distances (roughly a millimeter).

The steepness of the concentration gradients is better revealed by the high-resolution measurements. Fig. 4(b) shows a sample instantaneous concentration field taken on the centerline of the plume at five channel depths from the source. The individual filaments of the chemical tracer are now clearly observed and the highly intermittent nature of the plume is exhibited. The concentration rises from near zero to peak values of roughly $0.1 C_o$ over distances approaching the Batchelor scale. Molecular diffusion acts on these steep gradients, ultimately diluting and homogenizing the concentration field. Turbulent stirring continues to stretch and fold these filaments, continually creating very steep gradients.

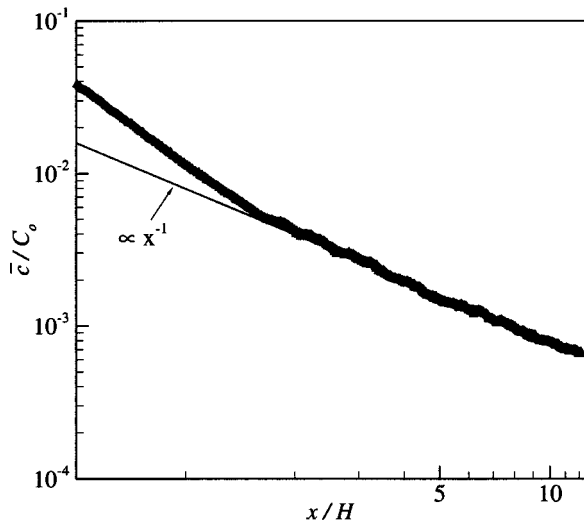


Fig. 5. Time-average concentration along plume centerline (data from four overlapping fields are shown)

Whereas the instantaneous concentration distribution demonstrates high spatial variability, the time-average and other statistical measures are expected to be smoother distributions. In fact, eddy diffusivity is often used to model the time-average concentration distribution. For a point release into a uniform flow with constant eddy diffusivity, the average concentration varies inversely with x (e.g., Fischer et al. 1979). The measured time-average concentration along the centerline of the plume is shown in Fig. 5. Close to the source (roughly up to $x/H=2$), the decrease in \bar{c} is faster than that predicted by the theoretical model. This is consistent with the idea that the eddy diffusion coefficient is not constant, but rather increases until the filament (or cloud) size grows to be larger than the largest eddy size (approximately $0.5 H$ in this flow). For $x/H > 2$, the average concentration along the centerline varies as the inverse of the distance from the source, which agrees well with the theoretical model.

Fig. 6 shows profiles of the time-average concentration in the spanwise direction at four downstream locations. Because the spanwise direction is essentially unbounded (i.e., the channel walls are very far away), the average concentration distribution is

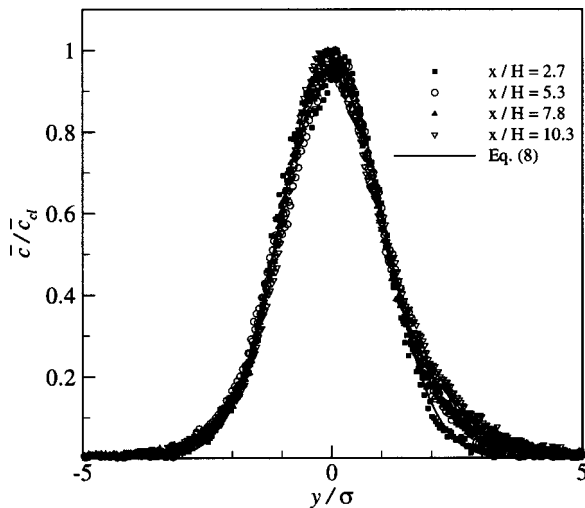


Fig. 6. Self-similar spanwise profiles of time-average concentration

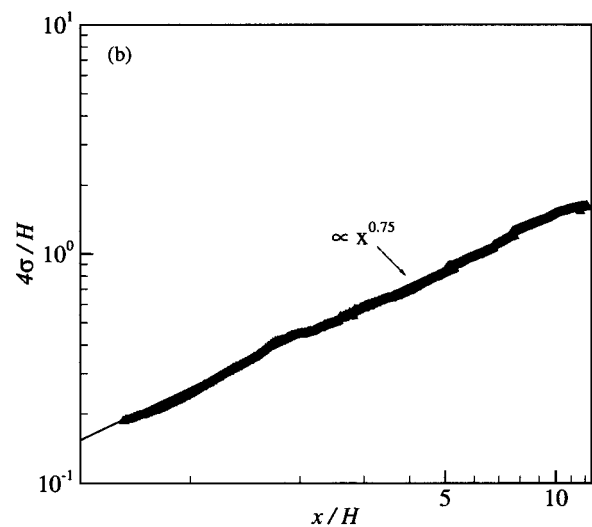
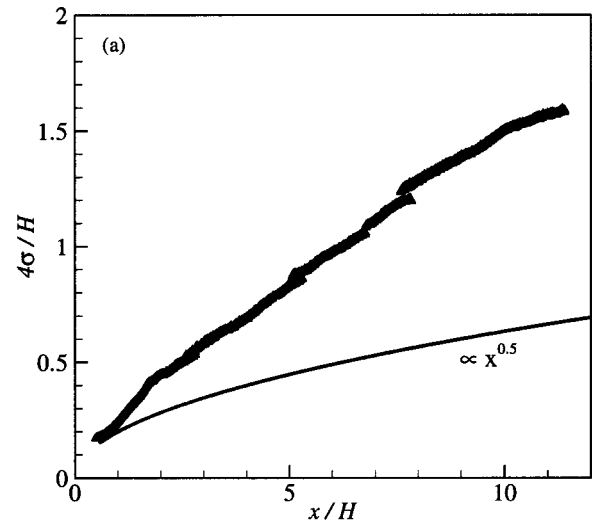


Fig. 7. Transverse plume width on (a) linear and (b) logarithmic axes

self-similar and shaped like a Gaussian profile. The standard deviation of the time-averaged profile, σ , and the centerline value of the average concentration are employed to demonstrate the self-similar profiles in Fig. 6. For these data, the Gaussian peak was assumed to be at the plume centerline ($y/H=0$), and the value of σ was determined from a linear regression between $\ln(\bar{c}/\bar{c}_{cl})$ and y^2 . Also shown in Fig. 6 is a Gaussian profile

$$\bar{c}(x, y) = \bar{c}_{cl}(x) \exp\left(-\frac{y^2}{2\sigma^2}\right) \quad (8)$$

As seen in Fig. 6, the measured profiles compare very well with the Gaussian profile.

The plume width is generally defined as four times the standard deviation of the time-averaged profile, σ . As expected, Fig. 7(a) shows that the transverse width increases as the plume evolves downstream. At $x/H=2$, the plume width roughly equals $0.5 H$, which matches the estimate of the size of the largest eddies in the flow. This observation is consistent with the fact that the turbulent transport appears to transition from relative to constant eddy diffusion around $x/H=2$, as just discussed regarding the average concentration profile (Fig. 5). The growth rate of the plume width, however, deviates significantly from the analytical prediction. The analytical solution of the advection–diffusion

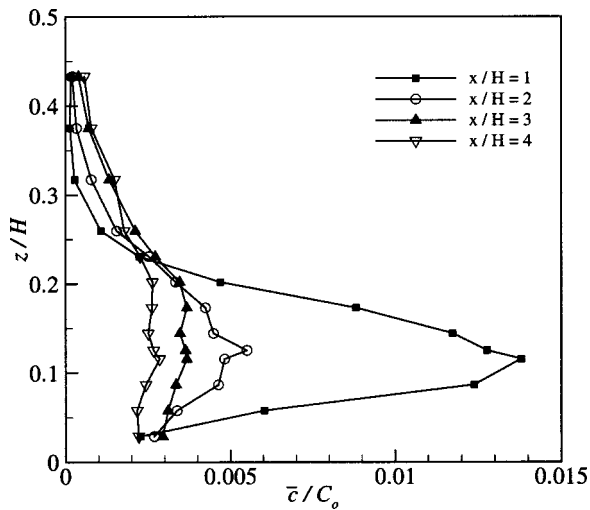


Fig. 8. Vertical profiles of time-average concentration

equation for a point release into a uniform flow with constant diffusivity predicts that the plume width increases in proportion to $x^{0.5}$ (e.g., Fischer et al. 1979). Fig. 7(a) includes a $x^{0.5}$ profile, and it is clear that the measured plume grows at a faster rate. The plume width plotted on logarithmic axes [Fig. 7(b)] shows that the profile follows a power law: $\sigma \propto x^{0.75}$.

Vertical profiles of the time-average concentration on the plume centerline are presented in Fig. 8 at four locations. For each profile, the peak value is near the release height of plume (i.e., $z/H = 0.125$). With distance from the source, the peak value decreases and the vertical profile becomes more uniform. The vertical distributions are not Gaussian due to the bounding influence of the bed. These data agree qualitatively with the elevated release data collected by Fackrell and Robins (1982) in a wind tunnel using a modified flame-ionization detector system.

Whereas the time-average concentration is often used when modeling turbulent chemical transport as a diffusion process, the time-average yields an incomplete, and possibly misleading, picture of an intermittent plume because it lacks any information about the fluctuations and peak values. The standard deviation (or variance) provides information about the magnitude of the concentration fluctuations. Fig. 9 shows vertical profiles of the standard deviation of the concentration fluctuations at four downstream locations. The vertical profiles for standard deviation have the same qualitative shape as those for time-average concentration (Fig. 8). The magnitude of the standard deviation for each profile is greater than the corresponding time-average, however. This indicates that the concentration fluctuates greatly about a relatively small time-averaged value, which agrees with the spatial variability (and hence, intermittency) observed in Fig. 4. As the plume evolves downstream, the fluctuation profiles decrease in magnitude and become flatter because the plume becomes more homogeneous. Again, the standard deviation profiles agree qualitatively with those presented by Fackrell and Robins (1982) in an airborne plume.

The fluctuations are expected to decrease with x as the concentration distribution becomes more homogeneous. According to a recent study of scalar fluctuations in a flow through a round pipe (Guilkey et al. 1997), the decay of scalar variance follows an exponential function in the near field and a power-law function in the far field. In the pipe flow experiment, the transition was around 35 pipe diameters downstream of the source, and Guilkey

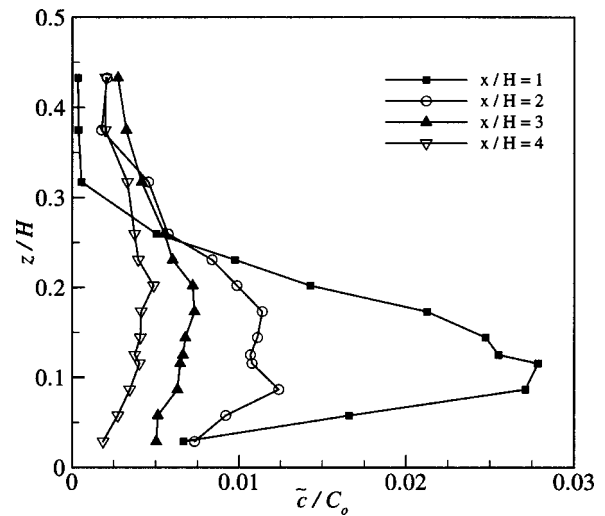


Fig. 9. Vertical profiles of standard deviation of concentration fluctuations

et al. (1997) reported that the power-law exponent varies from -2.4 to -3.3 . For the current data, the scalar fluctuations follow the same qualitative behavior (Fig. 10). Near the source, the variance decays exponentially as shown in Fig. 10 (x is scaled by the integral length scale of the velocity field, $H/2$, in the exponential function). Small-scale fluctuations in this region decay rapidly causing the variance to decrease exponentially. Beyond $x/H = 2$, the variance follows a power law with $n = -3.5$. In this region, large-scale fluctuations decrease more slowly, which yields a power-law decay of the scalar variance. For this power-law region, the variance (and standard deviation, $n = -1.75$) decreases faster than the time-average concentration (Fig. 5), which indicates the plume is becoming homogeneous faster than it is diluting. Finally, it should be noted that the data for $x/H < 2$ can also be fit well with a power law with an exponent of around -2 . The region is too short to definitively determine which functional form is correct from this single data set. We have plotted the exponential curve in order to compare with the theory and experiments of Guilkey et al. (1997).

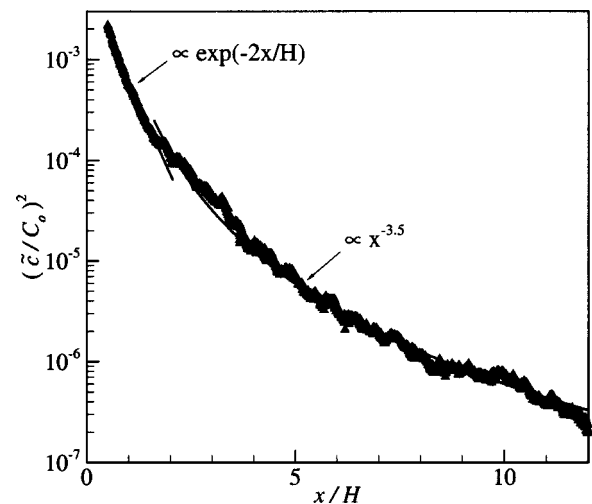


Fig. 10. Variance of concentration fluctuations along plume centerline

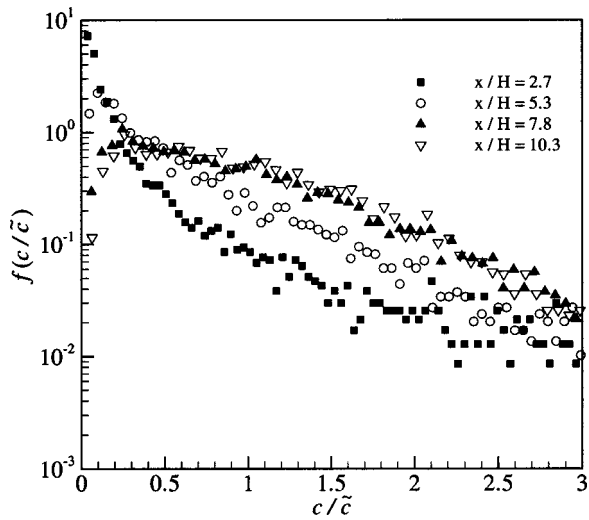


Fig. 11. Probability density function distributions of concentration at four locations on the plume centerline (measured concentration samples beyond $3\bar{c}$ are not shown)

The probability density function (PDF) of the instantaneous concentration for four locations on the centerline is shown in Fig. 11. The measured distributions do not resemble a Gaussian distribution. Instead, the distributions are highly skewed (skewness ~ 10) and very flat (kurtosis ~ 100). The distribution, even when normalized by the standard deviation, changes significantly with downstream distance. (Remember also that the value of the standard deviation decreases significantly with x , Fig. 10). At $x/H = 2.7$, the distribution indicates that there is a high probability of a zero- or near-zero concentration level. The tail extends well beyond three standard deviations, but such high concentration bursts are rare and the PDF in this range is difficult to resolve with a finite-length time record. With increasing distance downstream, turbulent mixing acts on the filaments and the probability of zero- or near-zero concentration decreases. Similarly, the probability of very high concentration samples (which are not shown) decreases. Conversely, the probability of fluctuations in the range of half to three standard deviations appears to increase. This shift in the distribution corresponds to the concentration field becoming more homogeneous as turbulent mixing acts on the filaments. At the farthest downstream locations ($x/H = 7.8$ and 10.3), a local maximum is observed in the PDF distribution around $c/\bar{c} = 0.5$. This suggests that as the filaments mix, concentration samples around $0.5\bar{c}$ are more probable than zero-concentration samples.

Conclusions

The LIF measurement technique is described in detail. The system consists of commercially available equipment including an argon-ion laser, rotating mirrors, a digital camera system, and computer-controlled timing. The procedure is summarized as follows. The rotating mirror sweeps the laser beam in a horizontal plane through the plume. Rhodamine 6G dye molecules absorb the laser light (green) and emit light at longer wavelengths (yellow-orange) with an intensity proportional to the concentration and laser sheet intensity. The emitted light is captured and recorded by the digital camera system. Using an *in situ* calibration, the raw images are converted to instantaneous planar concentration fields. A nonuniform sweep rate of the laser beam is

employed for the large-scale measurements because of the rapid dilution of concentration in the turbulent plume.

Concentration data are presented for an isokinetic chemical plume released into a fully developed turbulent boundary layer in an open channel flow. Measurements were performed for two image resolutions to demonstrate the range of scales of the concentration field. Because the flow is highly intermittent, long time records are required for statistical quantities, such as the time average, to converge (600 s for this plume). The average concentration measurements agree well with theoretical modeling and previous experimental observations for similar plumes. The transverse plume width increases as a power law with an exponent greater than that predicted by the idealized model. The variance of the concentration fluctuations appears to decrease as an exponential for $x/H < 2$ and as a power law with $n = -3.5$ beyond this point. This behavior agrees with the theory and measurements presented by Guilkey et al. (1997) for mixing in a turbulent pipe flow. The relative rate of decrease of the standard deviation compared to the average suggests that the plume is becoming homogeneous faster than it is diluting. The concentration PDF distribution is highly skewed and very flat and does not resemble a Gaussian distribution. The distribution physically corresponds to a concentration signal that is near zero with intermittent bursts of high concentration as individual filaments advect past the measurement location.

Acknowledgments

The writers gratefully acknowledge the valuable advice of Dr. Philip Roberts including that related to the nonuniform sweep rate analysis and calibration procedure. ONR/DARPA provided financial support for this project (Grant No. N00014-98-1-0776).

Notation

The following symbols are used in this paper:

- A = calibration slope;
- B = calibration intercept;
- C_o = source concentration;
- c = concentration;
- \bar{c} = time-average concentration;
- \bar{c}_{cl} = time-average concentration on plume centerline;
- \bar{c} = standard deviation of concentration fluctuations;
- D = molecular diffusivity;
- E = control voltage for rotating mirror;
- H = flow depth;
- I = intensity (gray scale) of pixel;
- i = pixel number in streamwise direction;
- j = pixel number in spanwise direction;
- L = length of optical path of laser beam;
- L_B = Batchelor length scale;
- l = integral length scale of velocity fluctuations;
- n = power-law exponent;
- Sc = Schmidt number;
- T = time period of laser sweep;
- t = time;
- u^* = wall shear velocity;
- \bar{u} = standard deviation of velocity fluctuations;
- \bar{u} = average velocity;
- v = Kolmogorov velocity scale;
- v = laser beam sweep velocity;

x = streamwise coordinate;
 y = spanwise coordinate;
 z = vertical coordinate;
 α = attenuation coefficient;
 γ = strain rate of smallest velocity scales;
 ε = dissipation rate;
 η = Kolmogorov microscale;
 ν = kinematic viscosity;
 σ = standard deviation of time-averaged spanwise profile;
 and
 τ = Kolmogorov time scale.

Subscripts

0 = starting voltage or position; and
 1 = end voltage or position.

References

- Arcoumanis, C., McGuirk, J. J., and Palma, J. M. L. M. (1990). "On the use of fluorescent dyes for concentration measurements in water flows." *Exp. Fluids*, 10, 177–180.
- Bara, B. M., Wilson, D. J., and Zelt, B. W. (1992). "Concentration fluctuation profiles from a water channel simulation of a ground-level release." *Atmos. Environ., Part A*, 26A, 1053–1062.
- Batchelor, G. K. (1959). "Small-scale variation of convected quantities like temperature in turbulent fluid. Part 1. General discussion and the case of small conductivity." *J. Fluid Mech.*, 5, 113–133.
- Borg, A., Bolinder, J., and Fuchs, L. (2001). "Simultaneous velocity and concentration measurements in the near field of a turbulent low-pressure jet by digital particle image velocimetry-planar laser-induced fluorescence." *Exp. Fluids*, 31, 140–152.
- Chen, D., and Jirka, G. H. (1999). "LIF study of plane jet bounded in shallow water layer." *J. Hydraul. Eng.*, 125(8), 817–826.
- Cowen, E. A., Chang, K.-A., and Liao, Q. (2001). "A single-camera coupled PTV-LIF technique." *Exp. Fluids*, 31, 63–73.
- Crimaldi, J. P., and Koseff, J. R. (2001). "High-resolution measurements of the spatial and temporal scalar structure of a turbulent plume." *Exp. Fluids*, 31, 90–102.
- Crimaldi, J. P., Wiley, M. B., and Koseff, J. R. (2002). "The relationship between mean and instantaneous structure in turbulent passive scalar plumes." *J. Turbulence*, 3(014), 1–24.
- Dahm, W. J. A., and Dimotakis, P. E. (1987). "Measurements of entrainment and mixing in turbulent jets." *AIAA J.*, 25, 1216–1223.
- Fackrell, J. E., and Robins, A. G. (1982). "Concentration fluctuations and fluxes in plumes from point sources in a turbulent boundary layer." *J. Fluid Mech.*, 117, 1–26.
- Ferrier, A. J., Funk, D. R., and Roberts, P. J. W. (1993). "Application of optical techniques to the study of plumes in stratified fluids." *Dyn. Atmos. Oceans*, 20, 155–183.
- Fischer, H. B., List, E. J., Koh, R. C. Y., Imberger, J., and Brooks, N. H. (1979). *Mixing in inland and coastal waters*, Academic, San Diego.
- Guilkey, J. E., Kerstein, A. R., McMurtry, P. A., and Klewicki, J. C. (1997). "Mixing mechanisms in turbulent pipe flow." *Phys. Fluids*, 9, 717–723.
- Karasso, P. S., and Mungal, M. G. (1997). "PLIF measurements in aqueous flows using the Nd:YAG laser." *Exp. Fluids*, 23, 382–387.
- Kolmogorov, A. N. (1941). "The local structure of turbulence in incompressible viscous fluid for very large Reynolds numbers." *Dokl. Akad. Nauk Arm. SSR*, 30, 301.
- Koochesfahani, M. M., and Dimotakis, P. E. (1985). "Laser-induced fluorescence measurements of mixed fluid concentration in a liquid plane shear layer." *AIAA J.*, 23, 1700–1707.
- Koochesfahani, M. M., and Dimotakis, P. E. (1986). "Mixing and chemical reactions in a turbulent mixing layer." *J. Fluid Mech.*, 170, 83–112.
- Law, A. W.-K., and Wang, H. (2000). "Measurements of mixing processes using combined digital particle tracking velocimetry and planar laser induced fluorescence." *Exp. Therm. Fluid Sci.*, 22, 213–229.
- Nezu, I., and Rodi, W. (1986). "Open-channel flow measurements with a laser Doppler anemometer." *J. Hydraul. Eng.*, 112(5), 335–355.
- Sakakibara, J., Hishida, K., and Maeda, M. (1997). "Vortex structure and heat transfer in the stagnation region of an impinging plane jet (simultaneous measurements of velocity and temperature fields by digital particle image velocimetry and laser-induced fluorescence)." *Int. J. Heat Mass Transfer*, 40, 3163–3176.
- Tennekes, H., and Lumley, J. L. (1972). *A first course in turbulence*, MIT Press, Cambridge, Mass.
- Tracy, H. J., and Lester, C. M. (1961). "Resistance coefficients and velocity distribution smooth rectangular channel." *Paper No. 1592-A*, Geological Survey Water-Supply, U.S. Government Printing Office, Washington, D.C.
- Webster, D. R., Roberts, P. J. W., and Ra'ad, L. (2001). "Simultaneous DPTV/PLIF measurements of a turbulent jet." *Exp. Fluids*, 30, 65–72.
- Webster, D. R., and Weissburg, M. J. (2001). "Chemosensory guidance cues in a turbulent chemical odor plume." *Limnol. Oceanogr.*, 46, 1034–1047.